Global Modeling of Magnetized Capacitive Discharges

Mark D. Carter, Dan Hoffman, Steve Shannon, *Member, IEEE*, Philip M. Ryan, and D. Buchberger

***Abstract*—Capacitive reactors for semiconductor processing must simultaneously balance many physical phenomena with engineering constraints to achieve the desired processing properties. Important phenomena include electromagnetic RF propagation, gas ionization, plasma heating, plasma transport, and nonlinear sheath effects. Constraints are driven by process uniformity, radical production, thermal control, and reactor-component lifetime. These phenomena and constraints are often modeled in isolation; however, in a real system, they can interact in ways that are not easily foreseen. It is highly desirable to have global models that can provide relatively quick feedback for the proposed modifications to these systems. While an approach based on fundamental physics models is highly desirable whenever possible, the system can quickly become too complicated for quick design evaluations. In this paper, we explore the interaction between several processes by combining fundamental physics models when reasonable, with simplified, heuristic, or even empirical models for processes that are difficult to model from first principles. The goal is to understand the interaction between these processes in a global system without becoming overly encumbered by details in the individual components of the model. We study the effects of static magnetic field on plasma transport and electromagnetic effects arising at high RF frequency. We also change the RF-coupled power and ionization efficiency in a simplified 2-D model geometry to contrast the various effects. We find that discharges with very high frequency and high plasma density can exhibit localized nulls in the RF fields caused by electromagnetic-propagation effects in the sheath region. We find that relatively low static magnetic fields can modify the radial-plasma density profiles. Good agreement is found between the radial-plasma profiles given by the model and those measured in an experiment where the currents in two concentric coils near the plasma are the only variables.**

***Index Terms*—Capacitance, electromagnetic analysis, electromagnetic coupling, electromagnetic fields, electromagnetic heating, electromagnetic measurements, electromagnetic propagation in absorbing media, electromagnetic propagation in anisotropic media, electromagnetic propagation in dispersive media, electromagnetic propagation in nonhomogeneous media, electromagnetic propagation in nonlinear media, electromagnetic propagation in plasma media, electromagnetic surface waves, magnetic confinement, magnetic field effects, magnetic fields, perpendicular magnetic anisotropy, plasma applications, plasma confinement, plasma control, plasma devices, plasma generation, plasma heating, plasma materials-processing applications, plasma measurements, plasma properties, plasmas, plasma sheaths, plasma waves.**

Manuscript received February 15, 2007; revised June 21, 2007.

M. D. Carter is with Ad Astra Rocket Company, Houston, TX 77058 USA (e-mail: Mark.Carter@adastrarocket.com).

D. Hoffman, S. Shannon, and D. Buchberger are with Applied Materials, San Jose, CA 94086 USA.

P. M. Ryan is with Oak Ridge National Laboratory, Oak Ridge, TN 37831 USA.

Color versions of one or more of the figures in this paper are available online at http://ieeexplore.ieee.org.

Digital Object Identifier 10.1109/TPS.2007.906124

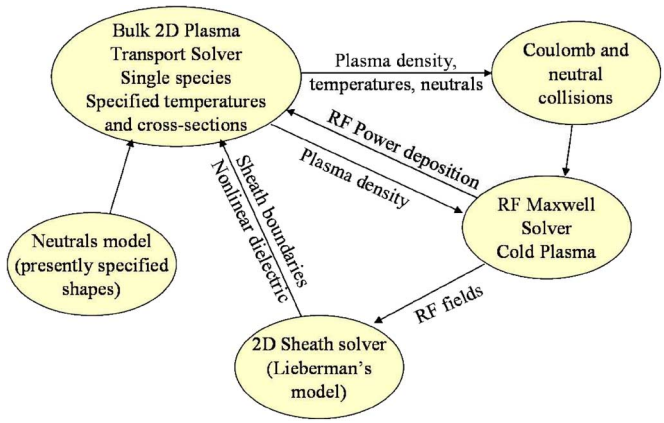

Fig. 1. Models for bulk-plasma transport, sheaths with finite thickness, and an electromagnetic model are iterated to obtain solutions in magnetized RF-generated discharges.

I. Introduction

STATIC magnetic fields affect the plasma-dielectric properties, plasma transport, and the distribution of electrons heated by the RF in capacitive discharges. Electromagnetic effects are important to consider for very high frequencies [1] under plasma conditions that produce thin highly capacitive sheaths. In this paper, we provide modeling results over a wide range of parameters to identify various physical effects (the 2-D model is described in detail in [2]). We also make a direct comparison between modeling and experimental results for the effect of magnetic fields on the radial-plasma density profile.

In the parameter study, the effects of magnetic field and sheath capacitance are shown in a simplified system for somewhat independently varying the RF power and energy cost for ionization to help isolate sheath and transport effects. We also vary the RF power, which changes both the sheath and density, at fixed ionization efficiency for frequencies of 13.56 MHz and 162 MHz. For the comparison with the experiment, good agreement is found between the plasma density profiles calculated by the model and ion-saturation current measurements from a movable Langmuir probe in an experiment designed to test magnetic-field effects in capacitive discharges.

A brief description of the model is reviewed in Sections II and III. A more detailed presentation of the model and assumptions therein can be found in [2]. As shown schematically in Fig. 1, the model combines an electromagnetic solver and a nonlinear-sheath model, which are described in Section II, with a diffusive transport model for magnetized plasma, which is described in Section III, where we also discuss a simplified analytic scaling of plasma transport with magnetic field. We

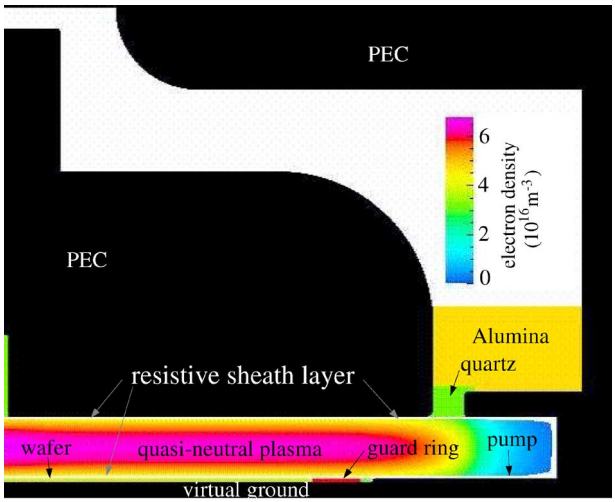

Fig. 2. Two-dimensional sheath model tracks the sheath thickness in r and z coordinates, using the previous iterates to determine the self-consistent sheath thickness. The thickness is based on a collisionless model using local values of the dependent quantities. The bulk plasma density inside the sheaths is determined by the transport model with the source obtained from the RF-power deposition in the RF model. The electrical circuit is assumed to provide a virtual ground at the wafer location. Note the short at the outer edge of the pumping port may affect results with relatively high magnetic fields.

use the model to compare the effects of plasma density and RF power at 13.56 and 162 MHz for the geometry shown in Fig. 2. For scale, the gap between the showerhead and the wafer is 30 mm for all of the modeling presented in this paper. Results from the model for various parameter dependencies are presented in Section IV to show different regimes in the model. A comparison between the model and experimental data is presented in Section V. Conclusions are presented in Section VI.

II. Electromagnetic Solution

The starting point for these calculations is a linear solution to the driven RF fields with magnetized plasma and finite sheath regions. Maxwell's equations

$$\nabla \times \vec{E} = i\omega\vec{B}; \quad \nabla \times \vec{B} = \mu_0 \vec{J}_{\text{ext}} - i\omega\epsilon_0\mu_0 \widetilde{K} \cdot \vec{E} \qquad (1)$$

are solved, where $\vec{E}$ and $\vec{B}$ are the complex RF electric- and magnetic-field vectors, respectively, with implicit $\exp(-i\omega t)$ time dependence, $\vec{J}_{\text{ext}}$ represents RF-current sources provided by an external generator, and $\widetilde{K}$ is a combination of the magnetized collisional cold plasma-dielectric tensor [3] and nonlinear-sheath losses [2].

Equation (1) is solved in cylindrical coordinates assuming azimuthal symmetry for the plasma properties so that Fourier analysis for the RF-field components is used only in the azimuthal direction. For this system, the RF drive is also symmetric in the azimuthal direction, so the Fourier decomposition need only consider the zeroth azimuthal mode. The numerical solution is obtained using finite-difference techniques in cylindrical coordinates with a staggered Yee grid.

Within a computational domain bounded by perfectly electrically conducting (PEC) surfaces with zero tangential electric field, additional PEC regions can be added to construct the driven (top) plate, the wafer-bias grid, and grounding connections leading to the edge of the domain. An axial RF current at the driving frequency is imposed across a small vacuum opening at $r = 0$ near the top of the model, as shown in Fig. 2, to generate the power source for the linear fields. Regions with scalar lossy dielectric properties are specified where they are desired to model the other components of the chamber. A static magnetic field is added using a filament model for coaxial circular coils. The plasma-dielectric-tensor properties are determined between the driven plates using the plasma distribution from the transport model, including neutral collisions, Coulomb collisions, and an *ad hoc* collision model to account for stochastic heating of electrons. A nonlinear dielectric is explicitly iterated in the solution to Maxwell's equations to describe the resistive dissipation in the sheath (this nonlinear model is described in more detail in [2]).

The model for the sheath is the collisionless analytic model of Godyak [4] and Lieberman [5]. RF electric fields obtained from the solution to (1) are integrated across the sheath and used to estimate the sheath thickness, which is then iterated with (1) and the transport model described below to close the scheme shown in Fig. 1.

III. Static Magnetic-Field Effects on Transport

Beginning with the continuity equation for the plasma inside the transport region assuming equal densities for electrons and singly charged positive ions,

$$\mathcal{S}(\vec{x}) = \nabla \cdot \Gamma_p(\vec{x}), \qquad (2)$$

where S is the net volumetric source rate for electron–ion production, and Γ_p is the quasi-neutral particle flux. We adopt a phenomenological model of the ionization source, based on the RF-power absorption per electron, to form an effective ionization-rate coefficient

$$S(\vec{x}) = \frac{\int_{V_i} P_{rf} d^3x'}{\int_{V_i} E_{\text{ion}}(\vec{x'}) d^3x'} \equiv n_e n_n \langle \sigma_{\text{ion}} v \rangle \qquad (3)$$

where V_i is a volume centered at $\vec{x}$ and extending over a region where heated electrons lose their energy as they scatter along their orbits, and E_{ion} is an average energy required for the creation of an electron–ion pair. The deposition volume V_i can be affected by magnetic fields which can change the region where heated electrons cause ionization. The quantity E_{ion} is primarily governed by radiation and ionization-energy losses and can be adjusted to account for losses in the system. As such, it can be used as a free parameter that is weakly dependent on details of the process so long as the supplied RF power is sufficient to sustain a discharge.

To obtain the flux $\Gamma_p(\vec{x})$ in two dimensions, we adopt a diffusive model for simplicity [2]. For a plasma with a single species of singly charged ions, the ambipolar-diffusion coefficient is given by

$$D_A = \frac{C_s(1 + T_i/T_e)}{n_n(\sigma_{en}\sqrt{m_e/m_i} + \sigma_{in}\sqrt{T_i/T_e})} \approx C_s L_i \qquad (4)$$

where n_n is the neutral-gas density, σ_{en} and σ_{in} are the total scattering cross sections with neutrals for electrons and

ions, respectively ($\sigma_{en} \sim$ a few 10^{-19} m^2, and $\sigma_{in} \gtrsim \sigma_{en}$), depending on the ion species, m_e is the electron mass, m_i is the ion mass, T_e is the electron temperature, T_i is the ion temperature, $C_s \equiv \sqrt{kT_e/m_i}$ is the ion-sound speed, and

$$L_i \equiv \frac{1}{n_n \sigma_{in}} \sqrt{\frac{T_e}{T_i}} \tag{5}$$

is the gradient scale length for the electrostatic potential.

The magnetic field can inhibit electron motion perpendicular to the field lines described by a cross-field diffusion coefficient D_ρ. The magnetization of the plasma determines D_ρ, which can be describe by classical diffusion for low magnetic-field strengths or by alternative diffusion models, such as Bohm diffusion, for higher field strengths. For the case of classical diffusion, the cross-field diffusion coefficient is given by

$$D_\rho \approx \frac{n_n \sigma_{en} v_{te}}{2} \rho_e^2 \tag{6}$$

where v_{te} is the electron thermal speed, and ρ_e is the electron gyro-radius. Transport across field lines is affected by the field when cross-field diffusion of electron gyro-orbits becomes smaller than the ambipolar diffusion, i.e., when $D_A \gtrsim D_\rho$. In the simplified case of $\sigma_{en} \approx \sigma_{in} = \sigma$, this condition occurs for classical diffusion when the typical collisional mean free path with neutrals $\lambda \equiv 1/(n_n \sigma)$ becomes greater than $\sqrt{\rho_e \rho_i/2}$, where ρ_i is the ion gyro-radius.

The magnetized and unmagnetized regimes are bridged to provide a continuous transition over a broad range of magnetic fields and pressures using

$$D_\perp \approx \frac{D_A D_\rho}{D_A + D_\rho} \qquad \text{and} \qquad D_\parallel \approx D_A \tag{7}$$

where the subscripts $\parallel$ and $\perp$ denote coordinates parallel and perpendicular to the field lines, respectively.

In a 2-D diffusion equation that uses an orthogonal coordinate system aligned parallel and perpendicular to the magnetic-field lines, (2) becomes

$$\mathcal{S}(\perp, \parallel) \approx -\frac{\partial}{\partial \parallel} D_\parallel \frac{\partial n(\perp, \parallel)}{\partial \parallel} - \frac{\partial}{\partial \perp} D_\perp \frac{\partial n(\perp, \parallel)}{\partial \perp} \tag{8}$$

where $\mathcal{S}(\perp, \parallel)$ is the local-source rate, and the operators are solved in a cylindrical coordinate system.

Where the plasma encounters a solid surface, nonlinear effects produce a sheath region. Plasma diffusion into the sheath region can be handled as a boundary condition for (8)

$$\left[D_A \frac{\partial n}{\partial \parallel} \right]_{\parallel_1} = -[C_s]_{\parallel_1} n_1; \quad \left[D_A \frac{\partial n}{\partial \parallel} \right]_{\parallel_2} = [C_s]_{\parallel_1} n_2 \tag{9}$$

where $\parallel_1$ and $\parallel_2$ denote the locations along a magnetic-field line, where the quasi-neutral plasma meets the sheath region. The values, n_1 and n_2, are the plasma densities at $\parallel_1$ and $\parallel_2$, respectively.

Changes in the plasma properties caused by magnetic fields may modify the RF power flow, but in cases where the RF absorption is nearly uniform, the predominant effect of a static magnetic field is to change the transport of the plasma. Under these conditions, insight into the physics of the model may be gained by inspecting an analytic estimate for the transport. For parameters such that $\lambda \gtrsim \sqrt{\rho_e \rho_i/2}$ and when there is a component of the magnetic field tangent to the parallel plates, plasma confinement can be enhanced. For coaxial magnet coils, the tangential component is the radial magnetic field. If the coil radius is greater than the plasma radius, field lines connect directly between the bottom and the driven top plate. For these parameters, the losses are mainly along field lines, and for weakly varying plasma and neutral parameters along a field line, the confinement time for a parabolic density distribution along the field line can be estimated by

$$\tau \approx \frac{L_c}{2C_s} \left(1 + \frac{L_c}{6L_i} \right) \tag{10}$$

where L_c is the connection length along the magnetic field lines between the plates. Modifications to transport are particularly important for plasma parameters, such that $L_c \gtrsim 6L_i$, where the factor "six" is a geometrical constant related to the assumption of a parabolic density profile along field lines.

For magnet-coil configurations that generate nearly straight field lines in the plasma region, the connection length between sheaths is roughly

$$L_c \approx L_G \sqrt{1 + B_r^2(r)/B_z^2(r)} \tag{11}$$

where L_G is the axial distance between the capacitor plates, and B_r and B_z are the radial and axial components of the magnetic field, respectively. Using (11) in (10) shows how confinement can be controlled over the radial extent of the plasma according to

$$\tau(r) \approx \frac{L_G}{2C_s} \left[\left(1 + \frac{B_r^2}{B_z^2} \right)^{1/2} + \frac{L_G}{6L_i} \left(1 + \frac{B_r^2}{B_z^2} \right) \right]. \tag{12}$$

The enhancement in confinement that can be gained by using a static magnetic field is given by $\bar{\tau} \equiv \tau(r)/\tau(r=0)$. Using (12), the fact that $B_r(r=0) = 0$ for coaxial magnet coils and further assuming that n_n, T_e, and T_i vary weakly in the radial direction, gives

$$\bar{\tau} \approx \left[\left(1 + \frac{B_r^2}{B_z^2} \right)^{1/2} + \frac{L_G}{6L_i} \left(1 + \frac{B_r^2}{B_z^2} \right) \right] \left(1 + \frac{L_G}{6L_i} \right)^{-1}. \tag{13}$$

The resulting enhancement is shown in Fig. 3.

A related modification occurs if the magnetic field is strong enough to guide heated electrons preferentially along field lines [2]. The transfer of heat by electrons becomes anisotropic in these regions so that heat supplied by the RF is redistributed along field lines in the discharge. This effect changes the density distribution by changing the ionization source $\mathcal{S}(\vec{x})$ in (3), rather than Γ_p.

IV. Parameter Variation

It is instructive to identify mechanisms in the model that allow changes to be controlled in a way that isolates different physical effects. In this section, we show the effects of variation

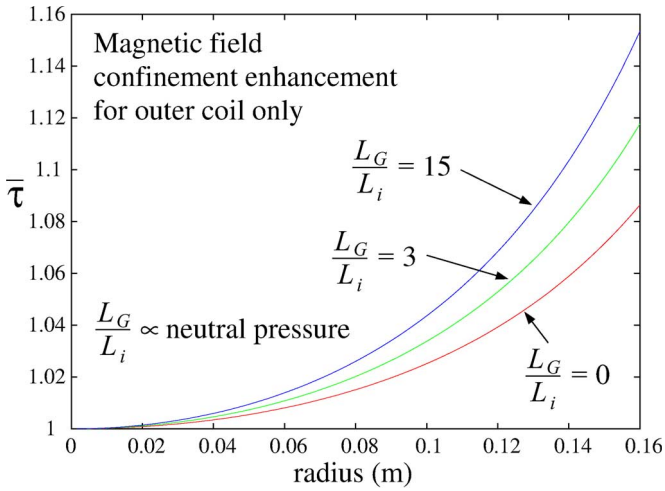

Fig. 3. For magnetic-field strengths and neutral-collision parameters such that electron transport is strongly guided along field lines, the radial component of the static magnetic field can significantly enhance confinement for plasma near the outer radius of the wafer.

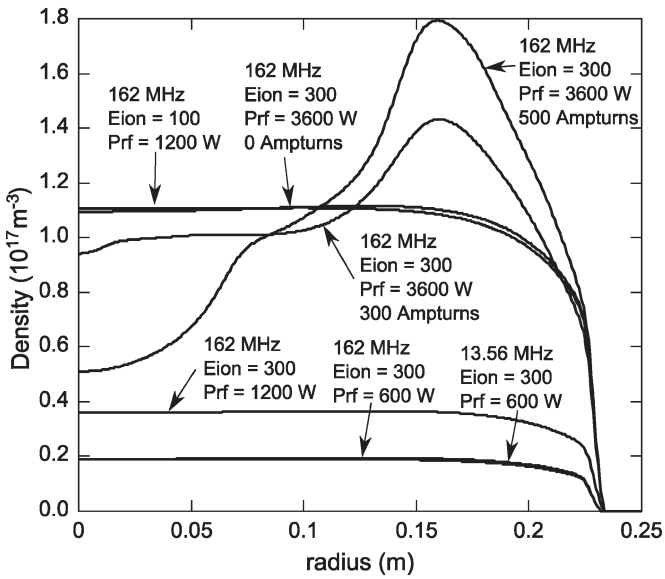

Fig. 4. Radial magnetic-field profiles from the transport model show the effects of varying the ionization efficiency $\propto 1/E_{\rm ion}$ for $E_{\rm ion} = 100$ and 300 eV and the applied RF power for 600, 1200, and 3600 W at 13.56 and 162 MHz. Results from the model for 13.56 MHz, with higher densities than the one shown, were not stable. The different magnetic-field settings, for a single coil just above the plasma at a radius of 16 mm, with $E_{\rm ion} = 300$ eV and RF power of 3600 W, show how the field moves plasma toward outer radii.

in the model's parameters without necessarily attempting to model any specific device. For these studies, the model illustrated in Fig. 1 was converged for several values of $E_{\rm ion}$ at different RF power levels P_{rf}, with and without magnetic fields produced by a single coil embedded in the top plate at a radius of 16 mm. The RF power is delivered to the top plate only. Increasing P_{rf} increases both the plasma density and the sheath voltage, so varying $E_{\rm ion}$ allows the bulk plasma density and the sheath thickness to be varied somewhat independently from the RF power. Similar variations in $E_{\rm ion}$ would be expected with different plasma chemistries. The radial density profiles for the various cases are shown in Fig. 4.

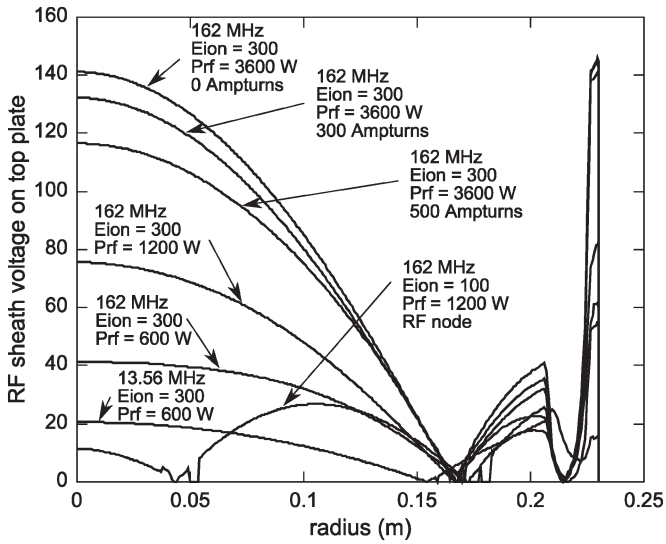

Fig. 5. RF voltage across the sheath at the top plate was weakly reduced by the magnetic field. The voltage is peaked on axis and drops monotonically over the region atop the wafer location for all of the cases shown except for the case of 162 MHz with $E_{\rm ion} = 100$ eV and RF power of 1200 W. For this high-frequency high-density low-power case, the sheath capacitance becomes large enough to form a propagation node in the fields, giving rise to a zero crossing in the RF sheath voltage on the top plate near a radius of 0.05 m.

Only a single low-density low-power case is shown for a driving frequency of 13.56 MHz, because parameters giving higher density typically make the ion-plasma frequency approach the driving frequency, so that the power does not efficiently penetrate the bulk plasma. For higher density cases at 13.56 MHz, excessive RF fields occur in the sheath region, preventing the sheath model from converging.

Two cases at 162 MHz, one with $E_{\rm ion} = 100$ eV and $P_{rf} = 1200$ W and the other with $E_{\rm ion} = 300$ eV and $P_{rf} = 3600$ W, show nearly identical density profiles in the absence of a magnetic field because the source rate, roughly proportional to $P_{rf}/E_{\rm ion}$, and transport conditions are nearly identical for these systems. The addition of 300 and 500 Amp turns (AT) in a single filament (just above the top plate at a radius of 16 mm) for $E_{\rm ion} = 300$ eV and $P_{rf} = 3600$ W caused the plasma density profile to change dramatically.

The RF voltages at the top (driven) plate for all these cases are shown in Fig. 5. The rise in RF voltage, with power on the top plate, is similar for all cases except for the 162-MHz case with $E_{\rm ion} = 100$ eV and $P_{rf} = 1200$ W. This high-frequency high-density low-power discharge produced a thin high-capacitance sheath along the top plate that allowed wave-propagation effects to cause a field node in the top sheath near a radius of 0.05 m.

The RF voltage on the bottom plate (not driven) is shown in Fig. 6. The fields on the bottom plate were only very weakly affected by the magnetic field and remained similarly peaked near the center for all cases. However, the profile is much more peaked for the high-density low- power 162-MHz case with $E_{\rm ion} = 100$ eV and $P_{rf} = 1200$ W because of propagation effects caused by the thin sheaths.

These results indicate that a static magnetic field can be used to significantly control the processing uniformity in these

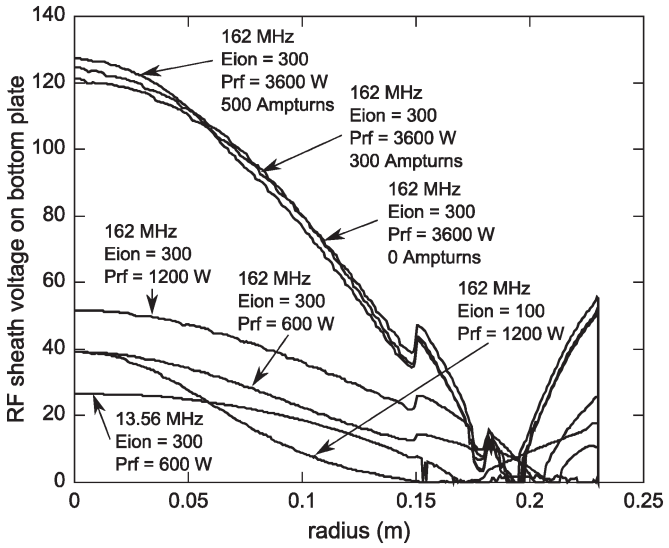

Fig. 6. RF sheath voltage along the grounded bottom plate remains peaked near the center for a wide range of parameters and is only weakly affected by the magnetic field. RF propagation effects give rise to a more strongly peaked voltage distribution on the bottom plate for the high-density low-power case at 162 MHz.

devices because of a change in plasma transport and RF-power deposition in the bulk of the plasma. They also show the importance of retaining electromagnetic effects when thin sheath conditions exist at high driving frequencies. The model was able to converge at significantly higher densities using 162 MHz as the driving frequency, rather than 13.56 MHz, because the ion-plasma frequency does not approach the driving frequency at 162 MHz at the power levels considered here.

V. Comparison With Experiment

Ion-saturation current data from a Langmuir probe in the proprietary charged species tuning unit experiment were made available for comparison with radial density profiles from the model for argon discharges using roughly 1200 W of RF power. The details of the actual configuration in the experiment are proprietary; therefore, the modeling was performed using a distorted simplified geometry with a small capacitive gap between the top portion of the pump plate, just below the alumina block, and the outer wall shown in Fig. 2. Parameters in the model were chosen to fit the experimental density profiles with no magnetic field, and these parameters were held fixed for comparison with data from magnetized discharges to see whether the observed experimental trends could be duplicated. The relevant parameters for the model are $E_{\rm ion} = 50$ eV, $T_e = 2.8$ eV, $T_i = 0.075$ eV, and 1200 W of total RF power to the plasma. The radial profile of the neutral gas density was also adjusted to provide a good fit with the unmagnetized data, as shown in Fig. 7. The functional used for the radial neutral-gas density profile was

$$n_{np} + n_{n0}\left[1 - \tanh\left((r - r_n)/r_s\right)\right]/2. \tag{14}$$

Such a distribution has not been measured but provides a means to study the effect of introducing gas from the showerhead while pumping away gas at the outer radii of the device. A good fit to the unmagnetized discharge data was obtained using crude estimates for the effective cross sections with $n_{np} = 8 \times 10^{19}$ m^{-3}, $n_{n0} = 4 \times 10^{20}$ m^{-3}, $r_n = 15$ mm, and $r_s = 25$ mm in (14). Near the center of the discharge, these parameters produce a mean free path for all electron collisions of $\sim$4 mm and a mean free path for all ion collisions of $\sim$2 mm. The model uses the algorithm described in [2] to determine the redistribution of RF power across field lines for ionization depending on the strength of the magnetic field. The mean free path for ionization in the absence of and along the direction of magnetic-field lines was $\sim$200 mm for these parameters. These mean-free-path lengths smoothly transition according to (14) to roughly double these values in the pump region for these parameters.

The only information provided for the geometry of the magnet coils in the experiment was that two coils were embedded near the surface of the showerhead somewhere above the plasma. An exhaustive study of the possible coil positions was not undertaken, but a reasonable fit to the data was obtained by assuming the same number of turns in each coil and placing two coils with 10-mm cross section 25 mm above the surface of the showerhead centered at radial locations of $r = 120$ and $r = 220$ mm. As shown in Fig. 7, this configuration in the model provided a good fit between the modeling and experimental results over a broad range of magnetic-field configurations.

The top plot in Fig. 7 shows the density profiles from both the model and experiment when no current was driven in the magnet coils. As previously discussed, the parameters in the model were adjusted to make the resulting density profile fit the experimental profile for the unmagnetized case, and a small capacitive gap was added in the pump region. Note the monotonically peaked radial profile in both the experiment and the model. After this initial fitting, all parameters except the currents in the magnet coils were kept the same for all of the plots shown in Fig. 7. In the second plot from the top, 400 AT were used in the model for the inner coil at $r = 120$ mm, and 0 AT were used in the outer coil at $r = 220$ mm; the result from the model is plotted along with the case from the experiment using 10 A on the inner coil only. Compared with the unmagnetized case, the profile shape for this case shows a mild depression in density near the center for both the model and experiment. In the third plot from the top, a current of -400 AT (opposite direction from the inner coil) was applied in the outer coil in addition to the 400 AT applied on the inner coil; this result shows little change from the unmagnetized case in both the model and experiment. In the bottom plot of Fig. 7, 400 AT were used in both the inner and outer coils (same direction); this result shows a significant hollowing of the plasma density profiles in both the model and experiment.

VI. Conclusion

Good agreement has been found between experimental measurements of radial-plasma density profiles and modeling for a wide range of different magnetic configurations where only the magnetic field was changed. Only very limited details concerning the power level and geometry of the proprietary

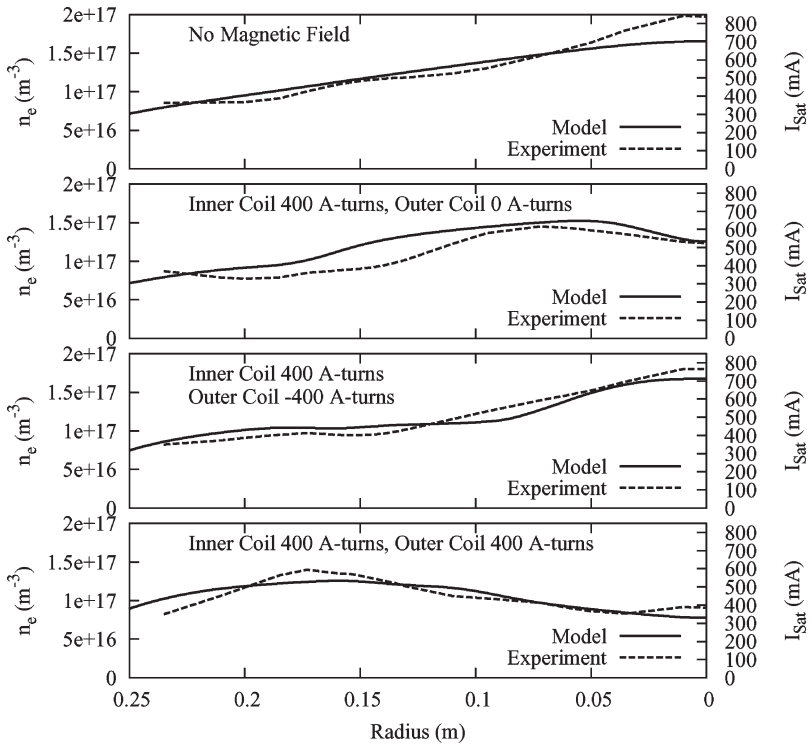

Fig. 7. To compare the model with experimental measurements, the model parameters were adjusted to fit the profile for the unmagnetized case in the experiment, as shown in the top plot. Except for the magnet currents, these same modeling parameters were used for all of the cases shown. The second plot (from the top) compares the density profiles from the model and experiment using the inner coil with only 400 AT in model and 10 A in the experiment. The third plot from the top shows the results of using $+400$ AT/ $+10$ A in the inner coil and -400 AT/ -10 A in the outer coil for the model/experiment. The bottom plot shows the results of using $+400$ AT/ $+10$ A in both coils for the model/experiment. The experimental variation was obtained by running repeated scans and reversing currents with roughly a 5% variation in results.

experimental device were provided, so parameters in the model were first adjusted to reasonable values that fit the unmagnetized data from the experiment. The comparison between experiment and model was then made for cases that involved only a change in the magnet-coil currents. The resulting model provides insight into the physics involved in the experiment using reasonable assumptions for the coil locations. The model relies on coupling relatively simple 2-D models for the electromagnetic response, the resulting RF sheath, the ionization source based on the deposition of RF power in the system, and the magnetized plasma transport. The model indicates that many of the effects caused by the addition of magnetic fields to these devices result from interactions between different processes. One significant process is the redistribution of RF power via heated electrons to modify the ionization along magnetic-field lines. A related effect is the reduction of the transport of plasma across magnetic-field lines after it is produced. Another important effect is the modification of the sheath capacitance that can lead to changes in the pattern of standing-wave electric fields for high-frequency sources. Proper modeling of these effects requires knowledge of the 2-D electrical connections both around and through the plasma.

ACKNOWLEDGMENT

Oak Ridge National Laboratory is managed by UT-Battelle, LLC, under Contract DE-AC05-00OR22725.

REFERENCES

[1] M. Lieberman *et al.*, "Standing wave and skin effects in large-area, high-frequency capacitive discharges," *Plasma Sources Sci. Technol.*, vol. 11, no. 3, p. 283, Aug. 2002.
[2] M. D. Carter, P. M. Ryan, D. Hoffman, W. S. Lee, D. Buchberger, and V. Godyak, "Combined RF and transport effects in magnetized capacitive discharges," *J. Appl. Phys.*, vol. 100, no. 7, p. 073 305, Oct. 2006.
[3] T. H. Stix, *Waves in Plasmas*. New York: Amer. Inst. Phys., 1992.
[4] V. A. Godyak, *1986 Soviet Radio Frequency Discharge Research*. Falls Church, VA: Delphic Associates.
[5] M. A. Lieberman, "Analytical solution for capacitive RF sheath," *IEEE Trans. Plasma Sci.*, vol. 16, no. 6, p. 638, Dec. 1988.

Mark D. Carter received the Bachelor's degree from the University of Missouri, Rolla, and the Ph.D. degree in nuclear engineering, specializing in plasma physics, from the University of Wisconsin, Madison.

He joined the Fusion Energy Division, Oak Ridge National Laboratory, in 1985, working on RF antenna design and plasma modeling for national and international fusion experiments. He has been a member of the Scientific Discovery through Advanced Computing-RF Team for the past several years and has recently begun applying modeling techniques to plasma-processing reactors. He joined the Ad Astra Rocket Company, Houston, TX, in 2006, where he currently leads the theory and computational modeling effort for the development of the variable specific impulse magnetoplasma rocket.

Dan Hoffman received the Bachelor's degree from the University of Pennsylvania, Philadelphia, and the Ph.D. degree in electrical engineering (plasma physics) from the University of Wisconsin, Madison.

He joined the Fusion Energy Division, Oak Ridge National Laboratory, in 1982, developing and leading plasma/RF research projects and programs for 16 years and establishing collaborations with French, German, Belgian, European Union, Japanese, and Korean research facilities, and large-scale fusion experiments at Princeton and San Diego. He also worked on RF and plasma systems for medical, semiconductor, waste management, and National Aeronautics and Space Administration applications. He joined the Etch Division, Applied Materials, San Jose, CA, in 1999, spearheading the development of a new high frequency plasma source that grew into the design and commercialization of the Enabler dielectric etcher.

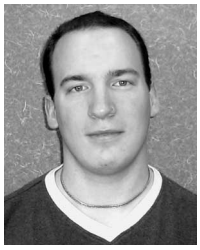

Steven Shannon (M'05) received the B.S.E., M.S.E., and Ph.D. degrees under the guidance of Prof. M. Brake and J. Holloway from the Department of Nuclear Engineering and Radiological Sciences, University of Michigan, Ann Arbor, MI, in 1995, 1997, and 1999, respectively.

He is currently a member of the technical staff with Applied Materials, Inc. and an Adjunct Professor with the Chemical and Materials Engineering Department, San Jose State University, San Jose, CA. In January of 2008, he will be joining the Nuclear Engineering Department, North Carolina State University, Raleigh, where he will continue his work in low-pressure plasma discharges. His research focus is in RF-plasma-source development for integrated-circuit fabrication and plasma diagnostics for characterization and control of process discharges. His current research focus is in multifrequency capacitive discharges.

Dr. Shannon is a member of American Vacuum Society and American Physical Society.

Philip M. Ryan received the B.S.E.E. degree from Michigan State University, East Lansing, in 1972, the M.S.E.E. from the University of Wisconsin, Madison, in 1973, and the Ph.D. degree in electrical engineering from the University of Tennessee, Knoxville, in 1986.

From 1997 to 2001, he managed the Plasma Chemistry Database and Modeling Research Program, SEMATECH, Austin, TX. Since 1974, he has been with Oak Ridge National Laboratory, where he is currently a Senior Research Staff Member with the Fusion Energy Division. His current fusion activities include the design, analysis, and application of high-power RF heating and current drive systems for tokamak experiments.

D. Buchberger, photograph and biography not available at the time of publication.